

Minimum grain size and compression mechanical behavior of polycrystalline graphene based carbon honeycombs: Cell irregularity and grain size effect

Jing-Jing Xing(邢静静), Shunran Liu(刘顺然), Ren-Liang Zhang(张任良), Yong-Gang Wang(王永刚), and Li-Jun Yi(易利军)

Citation: Chin. Phys. B, 2026, 35 (**7**): 076103. DOI: 10.1088/1674-1056/ae12d1
http://cpb.iphy.ac.cn; http://iopscience.iop.org/cpb

What follows is a list of articles you may be interested in

General-purpose moment tensor potential for Ga-In liquid alloys towards large-scale molecular dynamics with *ab initio* accuracy

Kai-Jie Zhao(赵凯杰) and Zhi-Gong Song(宋智功)
Chin. Phys. B, 2025, 34 (**6**): 066101. DOI: 10.1088/1674-1056/adc661

Anelasticity to plasticity transition in a model two-dimensional amorphous solid

Baoshuang Shang(尚宝双)
Chin. Phys. B, 2024, 33 (**1**): 016102. DOI: 10.1088/1674-1056/acf82c

Migration of weakly bonded oxygen atoms in a-IGZO thin films and the positive shift of threshold voltage in TFTs

Chen Wang(王琛), Wenmo Lu(路文墨), Fengnan Li(李奉南), Qiaomei Luo(罗巧梅), and Fei Ma(马飞)†
Chin. Phys. B, 2022, 31 (**9**): 096101. DOI: 10.1088/1674-1056/ac560f

Function of large-volume high-pressure apparatus at SECUF

Pinwen Zhu(朱品文), Qiang Tao(陶强), Lu Wang(王璐), Zhi He(何志), Tian Cui(崔田)
Chin. Phys. B, 2018, 27 (**7**): 076103. DOI: 10.1088/1674-1056/27/7/076103

Wettability of Si and Al-12Si alloy on Pd-implanted 6H-SiC

Ting-Ting Wang(汪婷婷), Gui-Wu Liu(刘桂武), Zhi-Kun Huang(黄志坤), Xiang-Zhao Zhang(张相召), Zi-Wei Xu(徐紫巍), Guan-Jun Qiao(乔冠军)
Chin. Phys. B, 2018, 27 (**4**): 046101. DOI: 10.1088/1674-1056/27/4/046101

Minimum grain size and compression mechanical behavior of polycrystalline graphene based carbon honeycombs: Cell irregularity and grain size effect

Jing-Jing Xing(邢静静)[1], Shunran Liu(刘顺然)[1], Ren-Liang Zhang(张任良)[2], Yong-Gang Wang(王永刚)[1], and Li-Jun Yi(易利军)[1,†]

[1] *Key Laboratory of Impact and Safety Engineering, Ministry of Education, School of Mechanics and Engineering Science, Ningbo University, Ningbo* 315211, *China*
[2] *School of Civil Engineering and Mechanics, Yanshan University, Qinhuangdao* 066004, *China*

(Received 20 July 2025; revised manuscript received 5 October 2025; accepted manuscript online 14 October 2025)

The graphene-based carbon honeycombs (CHCs) have excellent mechanical properties and various applications, and have attracted intensive attention recently. However, the real CHCs in experiments have random cell shapes. The effects of polycrystallinity and cell irregularity on the mechanical properties of CHCs are still unknown. Here, first, we investigate the minimum cell size stability with ideal cell walls in the polycrystalline graphene-based carbon honeycombs (PGCHs). Then, based on molecular dynamics simulations, the compressive mechanical properties of four PGCHs with typical cell irregularities are studied systematically, including the periodic regular graphene-based carbon honeycombs (RGCHs) with a zero-degree cell irregularity. Under in-plane compression, the Young's modulus, initial peak stress, mean plateau stress, and per volume energy absorption W_v of RGCHs and PGCHs decrease significantly with increasing grain size, and show a pseudo Hall–Petch relation. The mean plateau stress and W_v of PGCHs are higher than those of RGCHs. Under out-of-plane compression, the grain size effect is also obvious. However, the influence of cell irregularity is very small and can be ignored. The results indicate that the Hall–Petch relations of polycrystalline materials are dependent on both grain size and cell irregularity, and provide theoretical guidance for real CHCs in engineering applications.

Keywords: mechanical behavior, graphene-based carbon honeycombs, cell irregularity, grain size effect

PACS: 61.48.Gh, 62.20.Qp, 31.15.xv

DOI: 10.1088/1674-1056/ae12d1 **CSTR:** 32038.14.CPB.ae12d1

1. Introduction

Carbon honeycomb is a three-dimensional (3D) cellular structure consisting of graphene nanoribbons,[1] and attracts wide attention due to unique physical and chemical properties. Carbon honeycomb shows distinctive electronic and magnetic properties,[2–4] excellent mechanical properties,[5–9] high thermal conductivity.[8–11] It has excellent potential applications, such as high adsorption and storage capacity for gaseous and liquid species,[1,2,12] and excellent anti-impact energy absorption.[6,7,13] Carbon honeycomb may also possess potential applications in nanoscale resonators and heat transfer.[14–16] However, although the real carbon honeycomb is always in a polycrystalline structure state in experiment,[1,17] most previous studies are based on periodic regular graphene-based carbon honeycombs (RGCHs), except for the thermal conduction properties of polycrystalline graphene-based carbon honeycombs (PGCHs).[10] Grain boundaries and grain size can influence the mechanical properties of nanocarbon materials significantly.[18–20] However, it is still unclear about the effect of grain size and cell irregularity on the mechanical properties of PGCHs. The related work not only reveals various natural phenomena, but also has enormous application prospects in the emerging field of nanotechnology.

A comparative study of PGCHs and RGCHs can help us better understand their mechanical behavior and explore the related mechanism. Consider the cell in RGCHs as a grain. Its cell wall length is related to the grain size.[10] Meng *et al.*[7] found that the in-plane compression mechanical properties of RGCHs are mainly dependent on the grain size and the density of knots between graphene ribbons. Gu *et al.*[8] indicated that the mechanical properties of RGCHs under tension are dependent on the cell wall length. However, the cell wall length is less than ~ 2.0 nm, and the compressive mechanical properties of RGCHs affected by the cell size are not reported. Zhang *et al.*[5] demonstrated in-plane tension and compression mechanical properties of RCHs with different cell wall lengths. Xing *et al.*[21] proposed anisotropic and tunable mechanical properties of asymmetric carbon honeycombs by constructing various cell wall sizes, found that the famous Gibson–Ashby model fails to predict the mechanical properties of RGCHs, and developed a new useful mechanical model. A systematic study is required on the grain size effect on the mechanical

[†]Corresponding author. E-mail: yilijun@nbu.edu.cn

© 2026 Chinese Physical Society and IOP Publishing Ltd. All rights, including for text and data mining, AI training, and similar technologies, are reserved.

properties of RGCHs and the related mechanism, especially compared with the grain size effect on PGCHs.

In this study, to study the effect of grain size and cell irregularity, a method based on Voronoi mosaic technology to construct the PGCHs is constructed for comparison and mechanism analysis. Then, based on molecular dynamics simulations (MDs), we systematically study the mechanical properties of in-plane and out-of-plane PGCHs under compression. We focus on the following questions: What are the effects of the average grain size and cellular irregularity of PGCHs on their mechanical properties?

2. Methodology

The aperiodic structure of PGCHs is mainly realized by the Voronoi tessellation technique[10,22,23] with the Rhino software, which can construct random polycrystalline structures with various grain shapes. Figures 1(a)–1(c) show a typical geometry of RGCH with a zero-degree cellular irregularity. RGCHs are periodic arrays of honeycomb structures. The honeycomb wall is a single-layer graphene sheet (Fig. 1(a)). To form the honeycomb wall, the cell walls in the Voronoi diagram are replaced with armchair or zigzag-shaped graphene nanoribbons. The armchair junction is a six-membered ring structure (Fig. 1(e)), and the zigzag junction is a five–eight ring structure (Fig. 1(f)). The carbon atoms at the cell wall junction are marked in red (Figs. 1(e) and 1(f)). The cell structure of RGCHs is shown in Fig. 1(g). A parameter d (Fig. 1(d), not the h or l in Fig. 1(e)) is used to indicate the cell size for both PGCHs and RGCHs, which is the length between two seeds.[10] For RGCHs, there is a relation $h = l = d/\sqrt{3}$ in the simulation models. For example, taking the grain size d = $\sim$ 1.0 nm in zigzag RGCHs as an example, the parameters h and l are about 0.58 nm. In the simulations, the grain sizes of PGCHs are chosen from the minimum size to about 10.0 nm, which can well present the varying trend due to the size effect. The minimum cell size stability in PGCHs with different cell irregularities is presented in Subsection 3.1.

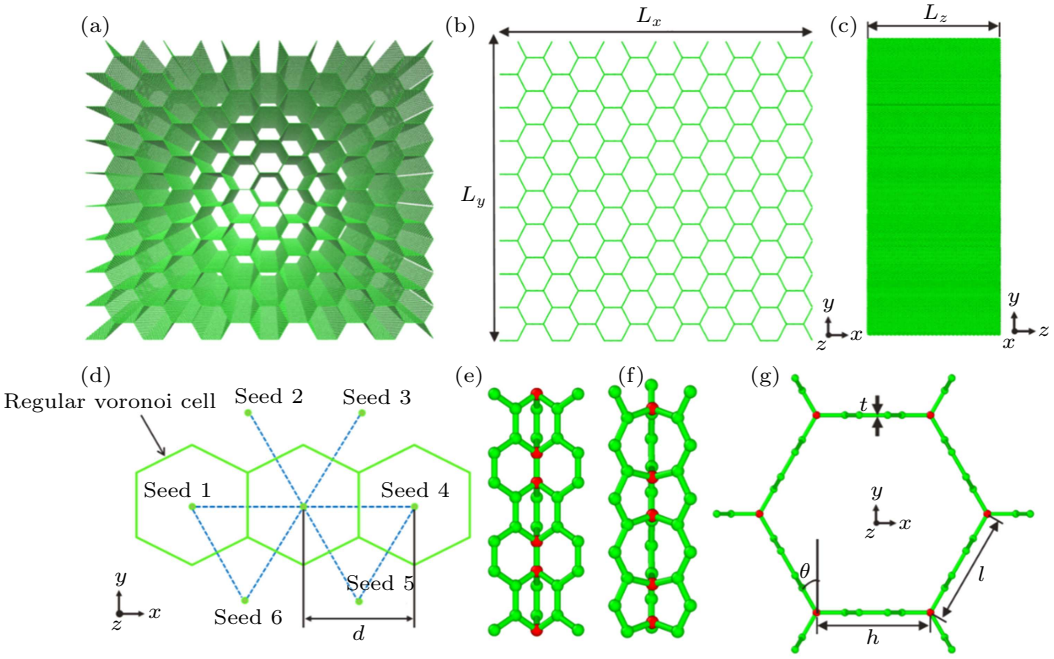


Fig. 1. (a) Geometry of an RGCH. Periodic boundary conditions are applied in all three directions. (b) Top view of the in-plane RGCH in x–y plane. (c) Side view of the out-of-plane RGCH in y–z plane. (d) Average grain size, where d is used to represent the cell size of both PGCHs and RGCHs, which is the distance between two regularly packed seeds. The atomistic structures of the junction composed of (e) armchair (six-membered ring structure) and (f) zigzag (five-eight ring structure) graphene nanoribbons. (g) Honeycomb cell.

The random features of PGCHs are acquired by the Voronoi tessellation technique. First, a set of seeds is placed in space simultaneously and randomly. Second, these random seeds grow with a uniform velocity in all directions. Then, depending on the space dimension, a two-dimensional (2D) or 3D Voronoi diagram is constructed. The Voronoi tessellation structure is fully determined by the initial locations of the seeds. Using regularly positioned seeds produces regular Voronoi diagrams. In order to construct a honeycomb structure with irregular cell shapes, a regular hexagonal honeycomb structure with a perfectly ordered, regular cell shape, and uniform cell wall length is first constructed, as shown in Fig. 2(a). Then, perturbations are introduced to the reference model to generate Voronoi diagrams with irregular cell shapes and nonuniform cell wall length.

The irregularity of cell shapes is determined by the irregular distribution of the seeds. The locations of the seeds used to construct Voronoi diagrams with irregular cell shapes are perturbed from a regular lattice of seeds. Figure 1(d) shows the coordinate perturbations of a regularly packed seed. The

perturbed coordinates (x_k, y_k) of the seed k can be represented by

$$x_k = x_k^0 + a(d\cos\theta_k)\varphi_k, \tag{1a}$$

$$y_k = y_k^0 + a(d\sin\theta_k)\varphi_k, \tag{1b}$$

where x_k^0 and y_k^0 are the two coordinates of the same seed in the regular lattice. d is the distance between two regularly packed (unperturbed) seeds. θ_k ($\in [0,\ 2\pi]$) is a uniformly distributed stochastic angle between the x_1-axis and the line connecting unperturbed and perturbed seeds. φ_k ($\in [-1, 1]$) is a random variable with a uniform distribution. a is the amplitude used to quantify the degrees of cell shape irregularity, and ranges between 0 and 1. The smaller a is, the more regular the Voronoi diagram is. Regular hexagonal honeycombs are obtained when $a = 0$, and completely irregular honeycombs are defined when $a = 1.0$. Figures 2(e)–2(h) show honeycomb samples with different degrees of cell shape irregularity. In the simulations, the degree of cellular irregularity of random PGCHs is chosen as 0, 0.2, 0.4, and 0.65. Figures 2(a)–2(d) show four Voronoi diagrams of PGCHs with (a) $a = 0$, (b) $a = 0.2$, (c) $a = 0.4$, and (d) $a = 0.65$ degrees of cell irregularity (with an average grain size of 3.9 nm). Then, models of PGCHs with (e) $a = 0$, (f) $a = 0.2$, (g) $a = 0.4$, and (h) $a = 0.65$ degrees of cell irregularity are obtained (Figs. 2(e)–2(h)). Graphene-based cellular carbon presents various styles, including multi-walled porous nanocarbons and composite nanoporous carbons composed of other molecules and materials.[24,25] The connectivity between the pores is diverse and even non-existent. Here, we only discuss the ideal honeycomb structure with a mono-layer thickness.[1] More typical simulation models of PGCHs, with average grain sizes of 6.01 nm and 9.88 nm, are shown in supplementary information S1.

The software package Lammps was used in the MD simulations. The structural analysis and processing were carried out by the visualization software OVITO. The binding interaction between the carbon atoms was described by the adaptive intermolecular reactive empirical bond order (AIREBO) potential.[26] The onset of the covalent interaction cut-off distance was set to 2.0 Å. The long-range van der Waals (vdW) interaction between carbon atoms was modelled by the Lennard–Jones potential with a well depth of 4.7483×10^{-22} J and an equilibrium distance of 0.3407 nm. The Nosé–Hoover thermostat was used to control the system temperature. The time step was taken as 1 fs.

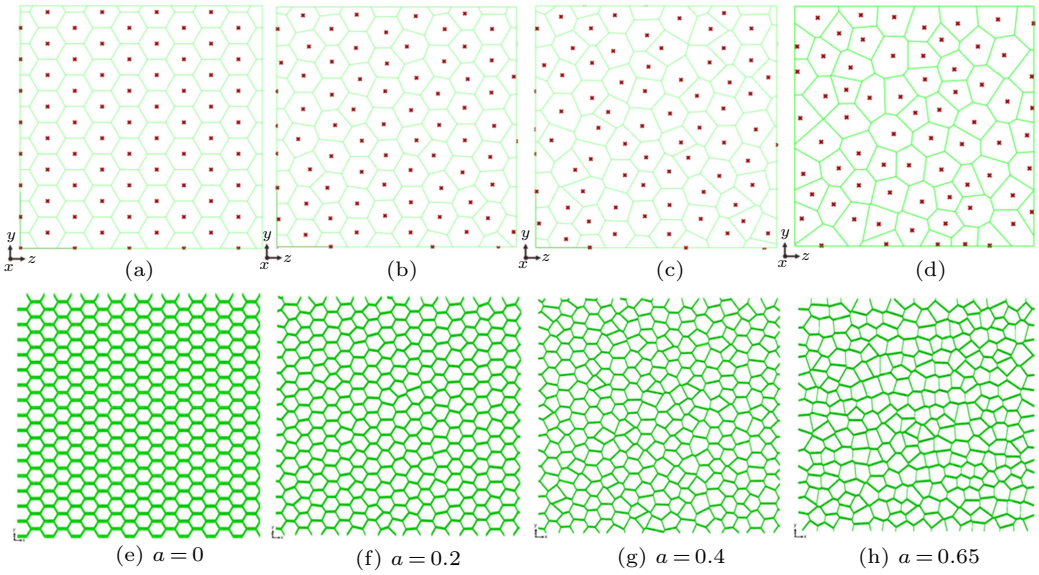


Fig. 2. Four Voronoi diagrams of 3.9-nm average grain size PGCHs are constructed with (a) $a = 0$, (b) $a = 0.2$, (c) $a = 0.4$, and (d) $a = 0.65$ degrees of cell irregularity. Four structural PGCHs with 3.9-nm average grain size are obtained with (e) $a = 0$, (f) $a = 0.2$, (g) $a = 0.4$, and (h) $a = 0.65$ cell irregularities.

In the in-plane simulations (loaded in the x–y plane), the side lengths L_x and L_y of PGCHs and RGCHs in the x and y directions were both set to ~ 60 nm, and the length L_z in the z direction was set to about 3.3 nm. Periodic boundary conditions were imposed in all three directions of RGCHs. Prior to the loading, the model was relaxed using the NPT ensemble until its energy was minimized at room temperature. Then an NVT ensemble was adopted to simulate the compressive behavior of PGCHs and RGCHs by applying a constant strain rate of 0.001 ps^{-1}. Young's moduli were calculated as the slope of the stress–strain curves $E = \sigma/\varepsilon$ at a small strain of 0.5%. The energy absorption per unit volume W_v and energy absorption per unit mass W_m at a specific strain ε are defined respectively as follows:[6,21]

$$W_\text{v} = \int_0^\varepsilon \sigma\,\text{d}\varepsilon \quad \text{and} \quad W_\text{v} = W_\text{m}/\rho, \tag{2}$$

where ρ is the mass density of GCHs.

In the out-of-plane simulations (loaded in the z direction), the side lengths L_x and L_y of PGCHs and RGCHs in the x and y directions were both about 7 nm, and the length L_z in the z

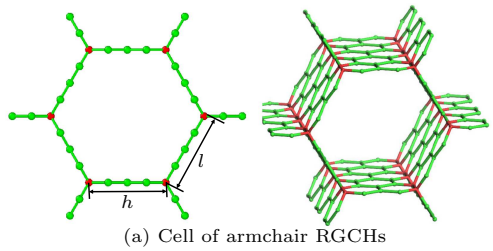
direction was about 10 nm. In the simulations, periodic boundary conditions were imposed in all three directions of RGCHs. In the calculation of the nominal stress of PGCHs and RGCHs, the cross-sectional area was defined as the product of the two side lengths in the x–y plane of PGCHs (Figs. 2(a)–2(d)). In the calculation of the real stress, the cross-sectional area was defined as the net area occupied by the graphene walls whose thicknesses were assumed to be 0.34 nm.

3. Results and discussion

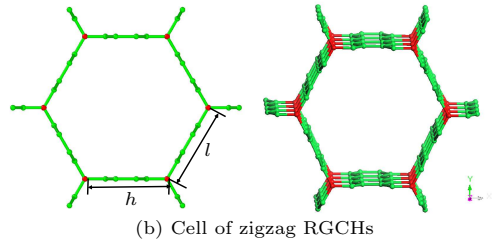
3.1. Minimum grain (cell) size in RGCHs and PGCHs with ideal cell wall

In symmetrical RGCHs, the cell wall height and length (h and l in Fig. 1(g)) equal $h = l$, and are different in asymmetric carbon honeycombs.[21] The Voronoi tessellation method in Section 2 can be used to construct any size of the height and length honeycomb cell wall. From the mathematical point of view, honeycomb with any small cell (grain) size is possible to build. However, physically, there are minimum cell (average grain) size for RGCHs and PGCHs, because that the cell walls of RGCHs and PGCHs are composed of graphene ribbons, and have minimum cell wall size h and minimum growth step sizes of cell wall Δh.

For RGCHs with the cell irregularity degree a of 0 (see Eq. (1)), as shown in Fig. 3, the minimum cell sizes $h_{\min}^{\text{arm}}$ and $h_{\min}^{\text{zig}}$ for armchair and zigzag symmetrical RGCHs are about 0.49 nm and 0.58 nm, respectively.[6] Otherwise, cell walls with smaller sizes are not ideal graphene ribbons. As mentioned in Section 2, there is a relation $h = l = d/\sqrt{3}$ between the cell wall and the average grain size d (Fig. 1(d)). Therefore, the corresponding minimum grain sizes $d_{\min}^{\text{arm}}$ and $d_{\min}^{\text{zig}}$ are ~ 0.85 nm and ~ 1.0 nm for armchair and zigzag RGCHs, respectively. In the following, we mainly use grain size d to describe PGCHs.



(a) Cell of armchair RGCHs



(b) Cell of zigzag RGCHs

Fig. 3. Minimum honeycomb cell of (a) armchair and (b) zigzag RGCHs with ideal cell wall.

The minimum average grain size of PGCHs is larger than $d_{\min}$ of RGCHs (PGCHs with $a = 0$). First, if the minimum average grain size of PGCHs is smaller than $d_{\min}$ of RGCHs, it means the cell wall does not consist of ideal graphene ribbons, because we already stated above that $d_{\min}$ is the smallest value for a cell wall to have ideal graphene ribbons. There should be some defects in the cell wall if the wall width is smaller than $d_{\min}$, and it is not the armchair or zigzag honeycomb structure which is defined in Fig. 1. Second, non-zero cell irregularity will induce perturbation of the grain size. If the minimum average grain size of PGCHs is equal to $d_{\min}$ of RGCHs with 0 degree cell irregularity, some cell wall widths should be smaller than $d_{\min}$, and some of them should be larger than $d_{\min}$, because the average of them is equal to $d_{\min}$. In the first case, we already stated that it is impossible for the minimum average grain size of PGCHs to be smaller than $d_{\min}$ of RGCHs. Therefore, the minimum average grain size of PGCHs is larger than $d_{\min}$ of RGCHs. In the following passage in this section, based on the analysis of the minimum grain size of RGCHs and the minimum growth step sizes of grain size, we will get the minimum average grain size $d_{\min}$ of PGCHs with 0.2, 0.4, and 0.65 cell irregularities.

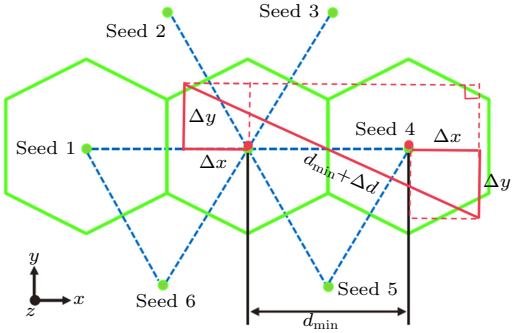


Fig. 4. The coordinates variation of the grain and the variation of the grain size.

The minimum growth step sizes of grain size for armchair (zigzag) symmetrical RGCHs is $\Delta d_{\min}^{\text{arm}} \approx 0.43$ ($\Delta d_{\min}^{\text{zig}} \approx 0.74$) nm. The average grain size increases as $d = d_{\min} + n \times \Delta d_{\min}$. Table 1 provides the cell wall size and average grain size of PGCHs with n from 0 to 7. As shown in Fig. 4, the grain size after variation based on $d_{\min}$ is

$$d_{\min} + \Delta d = \sqrt{(d_{\min} + 2\Delta x)^2 + (2\Delta y)^2}, \tag{3}$$

where Δx and Δy are the coordinates variation of the grain size. Based on Eq. (1), we choose the maximum variable value of $\sin\theta_k = \pm 1$, $\cos\theta_k = \pm 1$, and $\varphi_k = \pm 1$. Then, we can get Eqs. (4a) and (4b) to predicate the grain size after maximum variation of armchair and zigzag PGCHs respectively

$$(d_{\min} + \Delta d)_{\text{arm}} = \sqrt{(0.85 + 2a \times 0.85)^2 + (2a \times 0.85)^2}, \tag{4a}$$

$$(d_{\min} + \Delta d)_{\text{zig}} = \sqrt{(1.0 + 2a \times 1.0)^2 + (2a \times 1.0)^2}. \tag{4b}$$

For PGCHs with $a = 0.2$, using Eq. (4a), the grain size after variation of armchair PGCHs is $d_{\min} + \Delta d \approx 1.24$ nm. Therefore, the real minimum average grain size at least larger than 1.24 nm. Compared to Table 1, the real minimum average grain size should be 1.28 nm for armchair PGCHS with

$a = 0.2$. Similarly, using Eq. (4b), the grain size after variation of zigzag PGCHs is $d_{\min} + \Delta d \approx 1.46$ nm. Compared to Table 1, the minimum average grain size should be 1.74 nm for zigzag PGCHS with $a = 0.2$.

For PGCHs with $a = 0.4$, using Eq. (4a), the grain size after variation of armchair PGCHs is $d_{\min} + \Delta d \approx 1.67$ nm. Compared to Table 1, the minimum average grain size should be 1.71 nm for armchair PGCHs with $a = 0.4$. Similarly, using Eq. (4b), the grain size after variation of zigzag PGCHs is $d_{\min} + \Delta d \approx 1.97$ nm. Compared to Table 1, the minimum average grain size should be 2.48 nm for zigzag PGCHs with $a = 0.4$.

For PGCHs with $a = 0.65$, using Eq. (4), the grain size after variation of armchair PGCHs is $d_{\min} + \Delta d \approx 2.25$ nm. Compared to Table 1, the minimum average grain size should be 2.57 nm for armchair PGCHs with $a = 0.65$. Similarly, using Eq. (4b), the grain size after variation of zigzag PGCHs is $d_{\min} + \Delta d \approx 2.51$ nm. Compared to Table 1, the minimum average grain size should be 3.21 nm for zigzag PGCHs with $a = 0.65$. For convenience, Table 2 shows the minimum cell wall size and minimum average grain size of RGCHs and PGCHs with 0, 0.2, 0.4, and 0.65 cell irregularities.

Table 1. The cell wall size and average grain size of RGCHs and PGCHs with increasing step n from 0 to 7. The cell size and average grain size increase as $h = h_{\min} + n \times \Delta h_{\min}$ and $d = d_{\min} + n \times \Delta d_{\min}$, respectively. The minimum cell sizes and grain size for armchair (zigzag) symmetrical RGCHs are $h^{\text{arm}}_{\min} \approx 0.49$ ($h^{\text{zig}}_{\min} \approx 0.58$) and $d^{\text{arm}}_{\min} \approx 0.85$ ($d^{\text{zig}}_{\min} \approx 1.0$) nm, respectively. The minimum growth step sizes of cell wall and grain size for armchair (zigzag) symmetrical RGCHs are $\Delta h^{\text{arm}}_{\min} \approx 0.25$ ($\Delta h^{\text{zig}}_{\min} \approx 0.43$) and $\Delta d^{\text{arm}}_{\min} \approx 0.43$ ($\Delta d^{\text{zig}}_{\min} \approx 0.74$) nm, respectively. The relation between cell wall and average grain size d (Fig. 1(d)) is $h = l = d/\sqrt{3}$.

	$n = 0$	$n = 1$	$n = 2$	$n = 3$	$n = 4$	$n = 5$	$n = 6$	$n = 7$
h^{arm} (nm)	0.49	0.74	0.99	1.24	1.49	1.74	1.99	2.24
d^{arm} (nm)	0.85	1.28	1.71	2.14	2.57	3.0	3.43	3.86
h^{zig} (nm)	0.58	1.01	1.44	1.87	2.3	2.73	3.16	3.59
d^{zig} (nm)	1.0	1.74	2.48	3.21	3.95	4.69	5.43	6.17

Table 2. The minimum cell wall size and minimum average grain size of RGCHs and PGCHs with the increasing degree cell irregularity.

	$a = 0$	$a = 0.2$	$a = 0.4$	$a = 0.65$
$h^{\text{arm}}_{\min}$ (nm)	0.49	0.74	0.99	1.49
$d^{\text{arm}}_{\min}$ (nm)	0.85	1.28	1.71	2.57
$h^{\text{zig}}_{\min}$ (nm)	0.58	1.01	1.44	1.87
$d^{\text{zig}}_{\min}$ (nm)	1.0	1.74	2.48	3.21

As stated above, any small cell sizes of PGCHs are possible in mathematics based on the Voronoi tessellation method. We can contract PGCHs with smaller average grain size than the predicted minimum value. However, some cell walls in these conditions will not ideal graphene ribbons and have some defects. Take armchair PGCHs with 0.65 cell irregularity as an example. As shown in Fig. 5, we build $a = 0.65$ armchair PGCHs with 2.14-nm average grain size, which is smaller than the predicted minimum average grain size (2.57 nm) for armchair PGCHs with 0.65. As shown in Fig. 5, there are two types of defect walls. Type-I defect cell wall (Fig. 5(b)) is smaller than 0.25 nm. Type-II defect cell wall (Fig. 5(c)) is larger than 0.25 nm and smaller than 0.49 nm. Some defect walls may break after thermal relaxation and energy minimization. Even for the maintained structure stable, the cell wall structure is not PGCHs with ideal graphene ribbon cell wall. That is to say, it is not the ideal defined armchair or zigzag PGCHs in Fig. 1. Moreover, in the modeling process based on the Voronoi tessellation method, when one builds PGCHs with smaller average grain size and higher cell irregularity, more defects wall as shown in Fig. 5 will occur even if the building average grain size is larger than the critical value of the minimum average grain size. Therefore, to obtain ideal PGCHs with smaller average grain size and higher cell irregularity, more modeling iterations are required

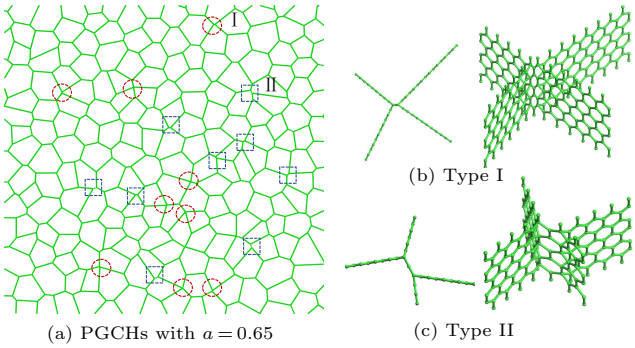


Fig. 5. PGCHs with defect wall. The cell wall is not ideal graphene ribbons in the defects. (a) An armchair PGCHs with $a = 0.65$-nm and 2.14-nm average grain size. (a) Type-I defect cell wall. (c) Type-II defect cell wall.

3.2. The x–y in-plane compression of zigzag PGCHs

3.2.1. The x-direction in-plane compression of zigzag PGCHs

The in-plane compression properties of honeycomb structures are a crucial concern in energy absorption in engineering design. Figure 6 shows the stress–strain curves of zigzag RGCHs and random PGCHs with different grain sizes under x-direction compression. The compression stress–strain curves of random PGCHs are consistent with those of RGCHs.[6,13,21] The stress–strain curves under x-direction compression show three ranges (Fig. 6): (I) the linear elastic stage, (II) the stress plateau stage, and (III) the densification stage. Compared to the macro-scale honeycomb, the densification stage in carbon honeycombs at the nano-scale actually includes an additional hardening stage due to the vdW interactions.[21,27] The detailed physical and mechanical significance of these stages

can be seen in our previous results.[6,13,21] The zigzag RGCHs and random PGCHs with smaller grain sizes have higher compression stresses under the same strain (Fig. 6). The compression stress decreases with increasing grain size, and the overall trend of the compression stress curve of PGCHs shows a pseudo Hall–Petch relation.[21]

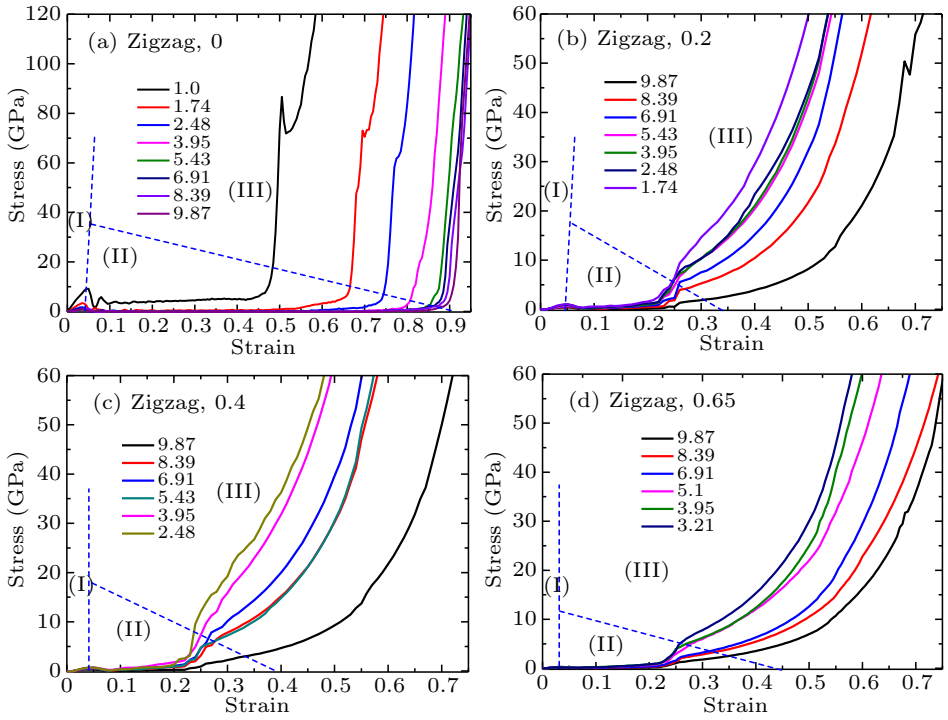


Fig. 6. Stress–strain curves of zigzag RGCHs and random PGCHs with (a) $a = 0$, (b) $a = 0.2$, (c) $a = 0.4$, and (d) $a = 0.65$ cell irregularities at different grain sizes under x-direction compression.

The Young's modulus, initial peak stress, mean plateau stress, and energy absorption per volume W_v in the linear elastic stage and plateau stage of zigzag RGCHs and random PGCHs decrease with increasing grain size (Figs. 7(a)–7(d)). As shown in Fig. 7(a), when the grain size increases from 1.0 nm to 9.8 nm, the Young's modulus of the zigzag RGCHs with 0 cell irregularity decreases from about 222.1 GPa to 26.2 GPa. When the grain sizes increase from 3.9 nm to 10.0 nm, the Young's modulus of zigzag random PGCHs with 0.2, 0.4, and 0.65 cell irregularities decreases from 38.3 GPa to 24.3 GPa, 27.6 GPa to 22.1 GPa, and 19.3 GPa to 17.2 GPa, respectively. As shown in Fig. 7(b), the initial peak stress of the zigzag RGCHs decreases from about 9.17 GPa to 0.51 GPa when the grain size increases from 1.0 nm to 9.8 nm. When the grain size increases from 3.9 nm to 10.0 nm, the initial peak stress of zigzag random PGCHs with 0.2, 0.4, and 0.65 cell irregularities decreases from 0.96 GPa to 0.42 GPa, 0.75 GPa to 0.33 GPa, and 0.31 GPa to 0.15 GPa, respectively. The smaller the grain sizes, the greater the density of the cell walls, which induces a more significant intensity of the vdW force between the cell walls. Hence, RGCHs and random PGCHs with a small grain size tend to have more tremendous stress under the same strain state.

According to Gibson–Ashby continuum model, the Young's modulus of honeycombs can be expressed as[21]

$$E_x = \left(\frac{t}{l}\right)^3 \frac{\cos\theta}{(h/l+\sin\theta)\sin^2\theta} E_g, \tag{5a}$$

$$E_y = \left(\frac{t}{l}\right)^3 \frac{h/l+\sin\theta}{\cos^3\theta} E_g, \tag{5b}$$

where E_x and E_y are the Young's modulus of honeycombs in the x- and y-directions, respectively, E_g is the Young's modulus of the honeycomb composition material. Here, for RGCHs, the cell length and height is equal to $h = l$, the cell width t is ~ 0.34 nm, and the angle is $\theta = 30°$. Therefore, we have

$$E_x \approx E_y \approx 0.091 \times E_g \left(\frac{1}{h}\right)^3. \tag{6}$$

According to our new model,[21] the Young's modulus of RGCHs in the x-direction and y-direction can be given by

$$E_x = \frac{t\cos\theta}{(h+l\sin\theta)} E_g, \tag{7a}$$

$$E_y = \frac{t(h+l\sin\theta)}{2l\cos\theta(h+l/2)} E_g. \tag{7b}$$

Substitution of $h = l$, the cell width t is ~ 0.34 nm, and the angle is $\theta = 30°$ into Eq. (7) yields

$$E_x \approx E_y \approx 0.196 \times E_g/h. \tag{8}$$

Using Gibson–Ashby model in Eq. (6) and our new model in Eq. (8) with $E_g = 600$ GPa,[6,20,21] we obtain the Young's modulus of RGCHs as compared in Fig. 7(a). Both models indicate the Young's modulus of RGCHs decrease with increasing cell size.

Graphene and CHCs show brittle fracture behavior under external loading.[6,21] According to the Gibson–Ashby continuum model, the brittle fracture stress of honeycombs can be expressed as[21]

$$(\sigma_{cr})_x = \frac{1}{3(h/l+\sin\theta)\sin\theta}\left(\frac{t}{l}\right)^2 \sigma_{fg}, \tag{9a}$$

$$(\sigma_{cr})_y = \frac{1}{3\cos^2\theta}\left(\frac{t}{l}\right)^2 \sigma_{fg}, \tag{9b}$$

where $(\sigma_{cr})_x$ and $(\sigma_{cr})_y$ are the fracture stresses of honeycombs in the x- and y-directions, respectively, σ_{fg} is the fracture stress of the honeycomb composition material. Substitution of the $h = l$, the cell width t is ~ 0.34 nm, and the angle is $\theta = 30°$ into Eq. (11) yields

$$(\sigma_{cr})_x \approx (\sigma_{cr})_y \approx 0.154 \times \sigma_{fg}\left(\frac{1}{h}\right)^2. \tag{10}$$

According to our new model,[21] the fracture stresses of RGCHs in the x-direction and y-directions are

$$(\sigma_{cr})_x = \frac{t\cos\theta}{(h+l\sin\theta)}\sigma_{fg}, \tag{11a}$$

$$(\sigma_{cr})_y = \frac{t}{2l\cos\theta}\sigma_{fg}. \tag{11b}$$

Substitution of $h = l$, the cell width t is ~ 0.34 nm, and the angle is $\theta = 30°$ into Eq. (10) yields

$$(\sigma_{cr})_x \approx (\sigma_{cr})_y \approx 0.196 \times \sigma_{fg}\frac{1}{h}. \tag{12}$$

Using the Gibson–Ashby model in Eq. (10) and our new model in Eq. (12) with $\sigma_{fg} = 80$ GPa,[6,20,21] we obtain the fracture stress of RGCHs compared with the initial peak stress in Fig. 7(b). Both models indicate that the initial peak stress of RGCHs decreases with increasing cell size.

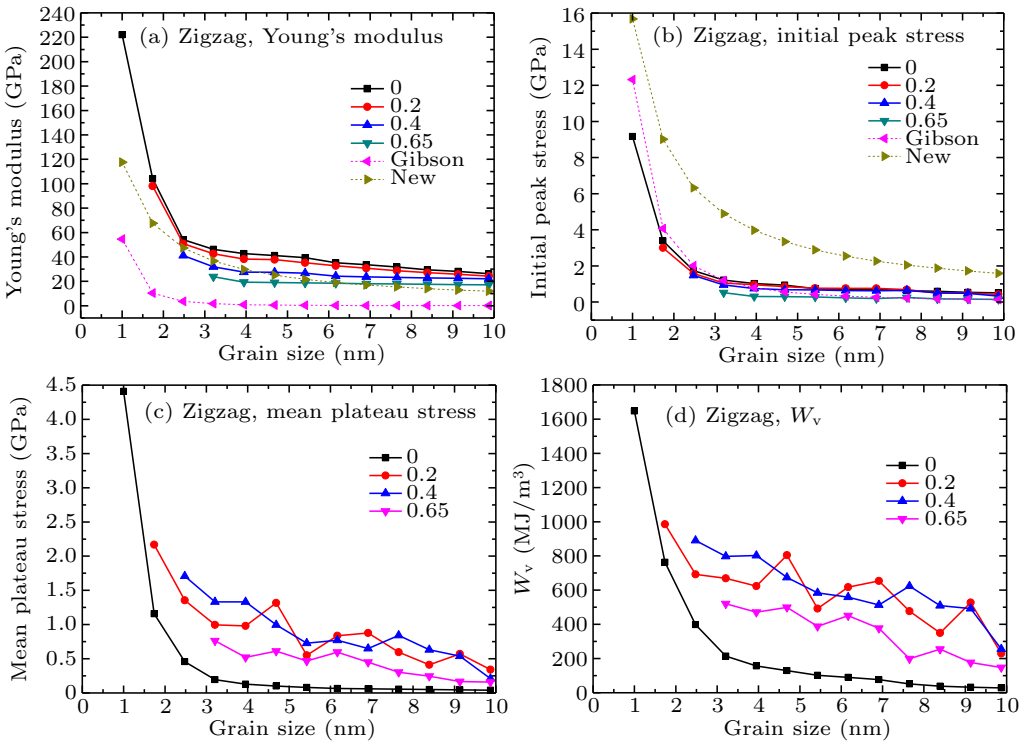


Fig. 7. (a) Young's modulus, (b) initial peak stress, (c) mean plateau stress, and (d) energy absorption per volume W_v of zigzag RGCHs and random PGCHs with different grain sizes under x-direction compression.

The mean plateau stress (Fig. 7(c)) and energy absorption per volume W_v (Fig. 7(d)) also decrease with increasing grain size over the whole varying trend. However, it should be noted that obvious fluctuations appear for random PGCHs, which may be due to the random and irregular grain structure. The mean plateau stress (Fig. 7(c)) and energy absorption per volume W_v (Fig. 7(d)) of PGCHs are higher than those of RGCHs. This means that random PGCHs can also be used as high-energy-absorption honeycomb materials.[6]

Why do the mean plateau stress and energy absorption per volume W_v of RGCHs and PGCHs decrease significantly with increasing grain size? The variation trends in W_v and mean plateau stress are nearly consistent (Figs. 7(c)–7(d)). The W_v is mainly determined by the zone of mean plateau stress. The plateau stress reflects the bending or compressive buckling and failure of the cell walls in the whole honey-

comb structure.[21] Short cell walls are more difficult to bend or buckle. Therefore, RGCHs with smaller grain size have higher plateau stress, and also have higher W_v.[21]

Why are the mean plateau stress and energy absorption per volume W_v of PGCHs higher than those of RGCHs? The average plateau stress and energy absorption are determined by the total effect of all cell walls. For a single cell wall, the cell wall strength is related to the cell wall size by a negative first power relationship as Eq. (12), or a negative second power relationship as Eq. (10). With the same average cell (grain) size h, RGCHs have a h cell wall, and PGCHs have some smaller $h-\Delta h$ and larger size $h+\Delta h$ cell walls. Taking two cell walls and Eq. (12) as an example, the strength of RGCHs is

$$0.196\times\sigma_{fg}\left(\frac{1}{h}+A\frac{1}{h}\right)=0.196\times\sigma_{fg}\frac{2}{h},$$

and the strength of PGCHs

$$0.196\times\sigma_{fg}\left(\frac{1}{h+\Delta h}+A\frac{1}{h-\Delta h}\right)\approx 0.196\times\sigma_{fg}\frac{2}{h-2\Delta h}.$$

Clearly, PGCHs have higher strength. Therefore, PGCHs have higher mean plateau stress and W_v than those of RGCHs. Theoretically, when the average grain size is the same, PGCHs with higher cell irregularity should have higher W_v. However, PGCHs in MD simulation are not infinite structures, and PGCHs with different degrees of cell irregularity under finite size cannot contain all random probabilities, so fluctuations of mean plateau stress W_v may occur (Figs. 7(c) and 7(d)).

3.2.2. The y-direction in-plane compression of zigzag PGCHs

The characteristic of the compression stress strain curves, Young's modulus, initial peak stress, mean plateau stress, and energy absorption per volume W_v in the linear elastic stage and plateau stage of zigzag PGCH under y direction in-plane tension is similar to those of zigzag PGCH under x direction in-plane tension. The detail results can be seen in the supplementary information S2.

3.3. The z-direction out-of-plane compression of zigzag PGCHs

Figure 8 shows the stress–strain curves of zigzag RGCHs and random PGCHs with different grain sizes under z direction compression. Figure 8 can be divided into four distinct phases, namely the alignment elastic phase (phase I), the buckling phase (phase II), the structural failure phase (also known as the plateau phase III), and the densification phase (phase IV). The detailed physical and mechanical significance of these phases can be seen in our previous work.[6,13,21] The compression stress of zigzag RGCHs and random PGCHs decreases with the increase of the grain size. The mechanization is that the smaller the grain size of the PGCHs, the higher the density of the graphene wall, and the net area of the honeycomb cell wall increases, and it can withstand more significant compression stresses.

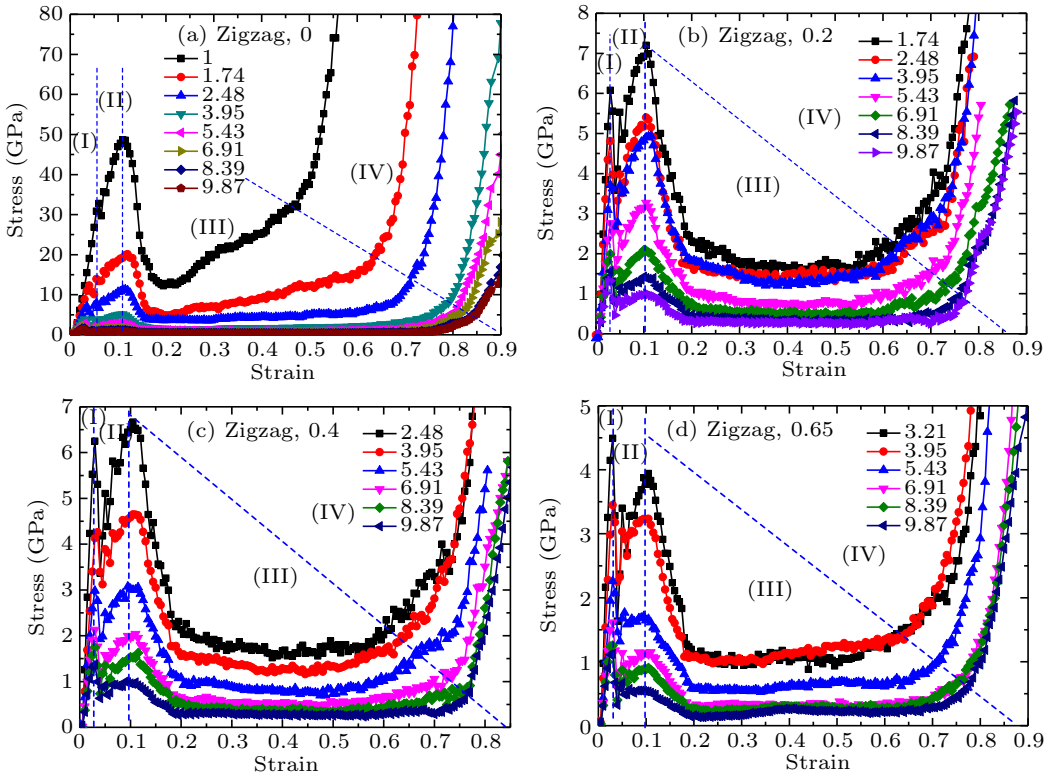


Fig. 8. Stress–strain curves of zigzag RGCHs and random PGCHs with (a) $a=0$, (b) $a=0.2$, (c) $a=0.4$, and (d) $a=0.65$ cell irregularities at different grain sizes under z-direction compression.

In Fig. 9, the Young's modulus, initial peak stress, mean plateau stress, and energy absorption per volume W_v of zigzag RGCHs and random PGCHs showed a decreasing trend with the increase of grain size. As shown in Fig. 9(a), the Young's modulus of the zigzag RGCHs decreases from about 661.7 GPa to 52.3 GPa when the grain size increases from 1.0 nm to 9.8 nm. When the grain size increases from 3.9 nm to 10.0 nm, the Young's modulus of zigzag random PGCHs with 0.2, 0.4, and 0.65 cell irregularities decreases from 142.1 GPa to 50.6 GPa, 157.8 GPa to 52.5 GPa, and 131.8 GPa to 35.1 GPa, respectively. As shown in Fig. 9(b), the initial peak stress of the zigzag RGCHs decreases from about 48.71 GPa to 1.25 GPa when the grain size increases from 1.0 nm to 9.8 nm. When the grain size increases from 3.9 nm to 10.0 nm, the initial peak stress of zigzag random PGCHs with 0.2, 0.4, and 0.65 cell irregularities decreases from 4.96 GPa to 1.01 GPa, 4.65 GPa to 0.99 GPa, and 3.23 GPa to 0.52 GPa, respectively. As shown in Fig. 9(c), the mean plateau stress of the zigzag RGCHs decreases from about 22.15 GPa to 0.52 GPa when the grain size increases from 1.0 nm to 9.8 nm. When the grain size increases from 3.9 nm to 10.0 nm, the mean plateau stress of zigzag random PGCHs with 0.2, 0.4, and 0.65 cell irregularities decreases from 2.03 GPa to 0.41 GPa, 2.0 GPa to 0.42 GPa, and 1.5 GPa to 0.29 GPa, respectively. As shown in Fig. 9(d), the W_v of the zigzag RGCHs decreases from about 10097.5 MJ/m^3 to 289.6 MJ/m^3 when the grain size increases from 1.0 nm to 9.8 nm. When the grain size increases from 3.9 nm to 10.0 nm, the W_v of zigzag random PGCHs with 0.2, 0.4, and 0.65 cell irregularities decreases from 1179.6 MJ/m^3 to 221.8 MJ/m^3, 1137.9 MJ/m^3 to 223.9 MJ/m^3, and 946.1 MJ/m^3 to 174.6 MJ/m^3, respectively.

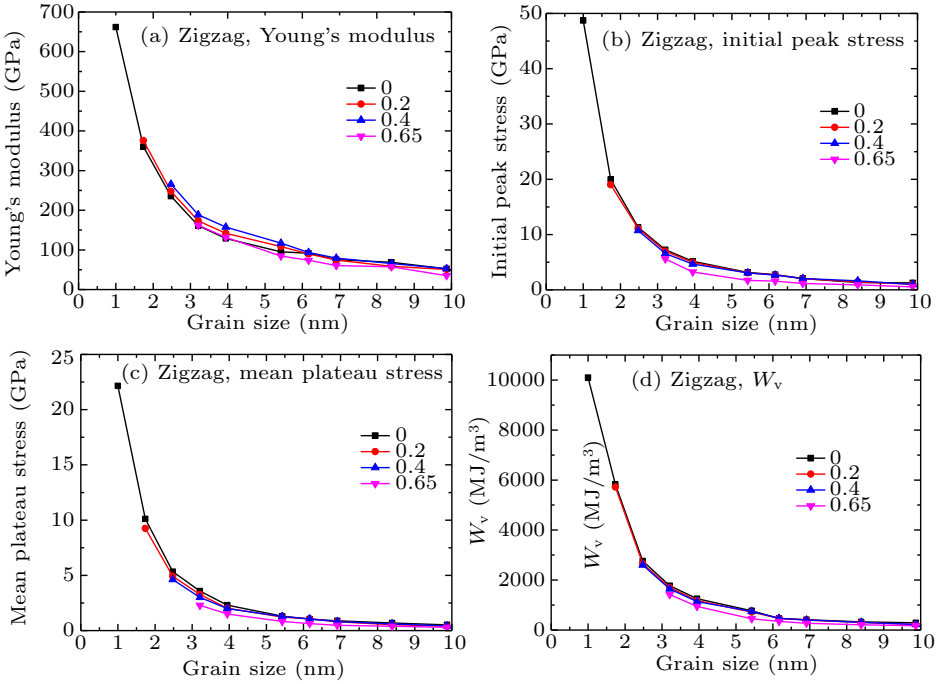


Fig. 9. (a) Young's modulus, (b) initial peak stress, (c) mean plateau stress, and (d) energy absorption per volume W_v of zigzag RGCHs and random PGCHs with different grain sizes under z-direction compression.

The effects of grain size and cell irregularity on the mechanical behavior of armchair RGCHs and random PGCHs can be seen in supplementary information S3. Armchair RGCHs and random PGCHs showed similar mechanical characteristics to the zigzag RGCHs and random PGCHs. Some deformation videos can be found in the attachments.

4. Conclusions

Based on theoretical analysis and MD simulations, the minimum stable grain sizes in RGCHs and PGCHs are studied. The related mechanism is that, physically, RGCHs and PGCHs have a minimum cell wall size and minimum growth step sizes of the cell wall, because the cell walls are composed of graphene ribbons. The mechanical properties of RGCHs and PGCHs are investigated under compression. Under in-plane compression, the Young's modulus, initial peak stress, mean plateau stress, and energy absorption decrease with increasing grain size overall, with some fluctuations. The mean plateau stress and energy absorption per volume of PGCHs are higher than those of RGCHs. Under out-of-plane compression, the Young's modulus, initial peak stress, mean plateau stress, and energy absorption decrease with increasing grain size. The grain size effect is obvious, but the irregularity effect is weak. This research can help predict the performance of future RGCHs and random PGCHs in engineering applications.

Acknowledgements

Project supported by the Ningbo Youth Science and Technology Innovation Leading Talents Project (Grant No. 2023QL021), the Fund from the National Key Laboratory of Shock Wave and Detonation Physics (Grant No. JCKYS2024212101), the Key Project of the National Natural Science Foundation of China (Grant No. U2530210), and the K. C. Wong Magana Fund through Ningbo University (NBU).

References

[1] Krainyukova N V and Zubarev E N 2016 *Phys. Rev. Lett.* **116** 055501
[2] Gao Y, Chen Y, Zhong C, Zhang Z, Xie Y and Zhang S 2016 *Nanoscale* **8** 12863
[3] Chen Y, Xie Y, Gao Y, Chang P Y, Zhang S and Vanderbilt D 2018 *Phys. Rev. Mater.* **2** 044205
[4] Yang Z, Lan G, Ouyang B, Xu L C, Liu R, Liu X and Song J 2016 *Mater. Chem. Phys.* **183** 6
[5] Zhang Z, Kutana A, Yang Y, Krainyukova N V, Penev E S and Yakobson B I 2017 *Carbon* **113** 26
[6] Yi L, Chang T, Feng X Q, Zhang Y, Wang J and Huang B 2017 *Carbon* **118** 348
[7] Meng F, Chen C, Hu D and Song J 2017 *J. Mech. Phys. Solids* **109** 241
[8] Gu X, Pang Z, Wei Y and Yang R 2017 *Carbon* **119** 278
[9] Pang Z, Gu X, Wei Y, Yang R and Dresselhaus M S 2017 *Nano Lett.* **17** 179
[10] Zhang J 2018 *Carbon* **131** 127
[11] Wei Z, Yang F, Bi K, Yang J and Chen Y 2017 *Carbon* **113** 212
[12] Zhou W, Xie H, Wang S, Wang Q and Jena P 2020 *Carbon* **168** 163
[13] Hu J, Zhou J, Zhang A, Yi L and Wang J 2021 *Phys. Lett. A* **391** 127130
[14] Zhang Y Y, Long M Q, Cheng S J and Zhou W X 2025 *Chin. Phys. B* **34** 067101
[15] Wang Y, Zhang Z, Wu C, Zhang Y, Lei G, Song X and Guo G 2025 *Chin. Phys. Lett.* **42** 070803
[16] Huang L, Ren K, Zhang H and Qin H 2023 *Chin. Phys. B* **32** 076103
[17] Krainyukova N V 2017 *J. Low Temp. Phys.* **187** 90
[18] Yue Z, Li J, Liu L and Mei H 2024 *Chin. Phys. B* **33** 086105
[19] Yan Y P, Zhang L T, Zhang L P, Lu G and Tu Z X 2024 *Chin. Phys. B* **33** 076201
[20] Yi L, Yin Z, Zhang Y and Chang T 2013 *Carbon* **51** 373
[21] Xing J, Wang Y, Yi Y and Zhang Y 2024 *Results Eng.* **24** 103296
[22] Zheng Z, Yu J and Li J 2005 *Int. J. Impact Eng.* **32** 650
[23] Li K, Gao X L and Subhash G 2005 *Int. J. Solids Struct.* **42** 1777
[24] Tong W, Zhang C, Zhang G, Pang K, Qin H and Liu Y 2025 *Adv. Mater.* **37** 2414410
[25] Luo S, Samad Y A, Chan V and Liao K 2019 *Matter* **1** 1148
[26] Stuart S J, Tutein A B and Harrison J A 2000 *J. Chem. Phys.* **112** 6472
[27] Li Y L, Tian Z G, Yin H F and Zhang R L 2024 *Chin. Phys. B* **33** 086103